Passive shock isolation utilising dry friction

M.I. Ismail, N.S. Ferguson

Institute of Sound and Vibration Research , University of Southampton, Southampton SO17 1BJ, UK

Abstract: A novel shock isolation strategy for base excited system is presented by introducing a two degree of freedom model with passive friction, where the friction is applied to an attached mass instead of directly to the primary isolated mass. The model is evaluated against the benchmark case of single degree of freedom system with friction applied directly to the primary isolated mass. The performance of the models are compared in term of the maximum displacement response and the acceleration during the application of the shock input for the case when the shock input duration is approximately equal to the natural period of the system (amplification region). From the results, the two degree of freedom model can produce both maximum displacement reduction and smoother acceleration at the point of motion transition. An experimental rig was built to validate the theoretical results against the experimental results; it is found that the experimental results closely match the theoretical predictions.

Keywords: Shock isolation, passive friction, two degree of freedom model, T-beam.

1. Introduction

Transient excitation or shock is a short duration input, which is often harmful because it typically involves high forces or motion that can subsequently produce high stresses and damage. The mechanical system response, due to the transient excitation, normally requires the time history of a quantity that describes the motion, typically the displacement, velocity or acceleration [1]. An inspection of the potential for damage can be made by prediction of the shock response spectra (SRS) [1]. For different types of pulses these SRS indicate the severity of the response when subjected to different pulse durations. The SRS can also assist in the choice and design of an isolation system [2]. Commonly, the analysis of shock isolation is performed using a single degree freedom system (sdof) model comprising linear elements subjected to different step and pulse functions [3].

Ramirez [4] describes and identified, for an undamped base excited single degree of freedom system, three regions of response; the isolation region where the maximum response is much smaller than the amplitude of the base input (when the pulse length is much smaller than the natural period of the system), the amplification region where the maximum response is larger than the amplitude of the base input (when the pulse length is approximately equal to the natural period of the system) and the quasi static region where the response follows the base input (when the pulse length is much larger than the natural period of the system.

A shock isolation system needs to be reliable mechanical design which could sustain different levels of shock excitation. A linear vibration or shock isolator is often used, typically comprising of an elastic element acting in parallel with a damping element, normally inserted between the existing structure and supporting structure and implemented in a very simple way without modifying the existing structure. The study by Hyun, Waters et al [5, 6] shows that such an isolation system with a viscous damper could transmit high forces during a shock for a sdof system subjected to base excitation.

This paper considers a passive isolation system, where friction is introduced as an alternative to the viscous damping element. Ideally it might limit the transmitted force, because its restoring force is not dependent on the magnitude of the relative velocity between the structure and the base. Early work by Hartog [7,8] and Hundal [9] in the modelling of friction examined various mechanical systems. Ferri [10] reviewed the relevant literature on the use of dry friction in passive damping and vibration isolation. Several analytical techniques were presented [10], with applications of dry friction in various areas and it was found that dry friction plays an important role.

Shock typically consists of two phases, the first phase is the response during the shock input application and second phase the residual vibration after the shock. In this paper, the strategy of interest for the first phase is to attenuate the response during the shock. The second phase to suppress the residual vibration after the shock was studied and discussed theoretically [11]. However, no experimental verification has been done and it may be interesting topic for future research. There are not many studies which concern the residual energy after the shock, where most studies only concern the forced response during the shock. The most related research came in the form of the free vibration analytical solution of a single degree of freedom system with friction, given by Timoshenko et al [12].

Among the first studies of a shock isolator configuration containing Coulomb friction is the work by Mercer et al [13]. They realized that Coulomb friction has a quality in that it can limit the acceleration transmitted to a mounted mass, which cannot be obtained using a viscous damper. In an adaptive configuration, for which the normal force is taken as a function of the displacement, this allows for the possibility of minimising the maximum displacement whilst still limiting the maximum acceleration. An optimum isolator is then a single degree of

freedom system where an elastic linear spring is in parallel with a series combination of a variable Coulomb friction element and a linear viscous damper [13]. When the motion is dominated by high frequency content, the viscous damper is locked as a rigid link and the isolator behaves as a spring with the Coulomb friction acting in parallel. Then, when the input motion becomes less severe, Coulomb friction becomes less dominant, less relative motion across it and viscous damping takes over to dissipate energy and restore the isolator to its equilibrium position. Because of good isolation property, there are a significant number of studies recently incorporating friction damping in the system for seismic isolation, for example [14, 15, 16]. The study by Castaldo *et al* employs a two degree of freedom model to represent the building flexing on the base mass [16]. Gaul *et al* also presented the two different semiactive control concepts for vibration reduction that adapt the normal force of attached friction dampers [17]. They compared simulation and experimental results of passive and semiactive controlled friction with stationary narrowband excitation.

Although Coulomb friction can minimise the maximum displacement, there is an issue with the acceleration response and an abrupt jump every time the motion starts and changes direction due to discontinuity of the Coulomb friction model. Therefore, a better shock isolation strategy for a base excited system is to apply friction at an attached mass instead of directly to the primary mass [11]. This paper will present and discuss this unique model and it will be evaluated against the benchmark case of single degree of freedom system with friction applied directly to the primary mass. Finally, to validate this strategy, an experimental rig was built and the theoretical results are compared with the experimental results.

2. Friction model

Friction is generally highly stochastic in nature [18]. Friction between sliding surfaces occurs a result of stochastic interactions between rubbing asperities. Various approaches to model the friction are presented in the literature, e.g.[19,20]. In nearly all cases there are significant variations in both amplitude and frequency, but most friction models do not take these variations into account and instead represent friction by a smooth mean value which is sufficiently accurate in term of the results for a dry friction system. The Coulomb friction is a piecewise linear function. Hence, the systems incorporating Coulomb friction are composed of segmented solutions and depend upon the direction of motion.

A Coulomb friction model used to simulate friction behaviour in this paper can be formulated as:

$$F = \begin{cases} F_c sgn(v) & if\ v \neq 0 \quad (2.1) \\ F_{st} & if\ v = 0\ and\ F_{st} \leq F_c \quad (2.2) \end{cases}$$

where F_{st} is the static friction force that the system has to overcome before the system can undergo relative motion. F_c is the sliding friction force defined as $F_c = \mu_c N$, μ_c is the coefficient of kinetic friction and N the normal load in contact. v is the velocity of the mass and the sign function $sgn(v)$ is often written as

$$sgn(v) = \begin{cases} +1 & for\ v > 0 \quad (2.3) \\ -1 & for\ v < 0 \quad (2.4) \end{cases}$$

A smooth function had been used herein to replace the sign function in the numerical implementation and solution of the governing differential equations of motion for easier and simpler computation. The smooth function used in this case is the error function, erf [21]. This function resembles the sign function closely, except that there is no discontinuity at $\dot{x} = 0$. How close the error function is to the sign function is governed by a constant 'a' which controls the smoothness of the error function curve. Some papers exist examining what is the appropriate value for the constant 'a', for example [20, 22]. In the papers, it is mentioned that a value of $a \geq 1000$ suffices to fit within the analytical solution within 1%.

In some cases, it has been found that the Coulomb friction model with the coefficient of static friction equal to dynamic or kinetic friction gives a good agreement to the validation experiment performed by Lopez *et al* within 10% [22]. This friction model is expected to give realistic predictions of the performance of friction damper with stiff / rigid localised contacts and large relative displacement within the contacts.

3. Benchmark case of a single degree of freedom system with friction

The typical model used to evaluate the performance of friction damping in shock isolation is a single degree of freedom model where friction is applied directly to the primary mass *m* as shown in **Figure 1** [11]. This model serves as a benchmark to the performance of the two degree of freedom model which will be introduced in the next section.

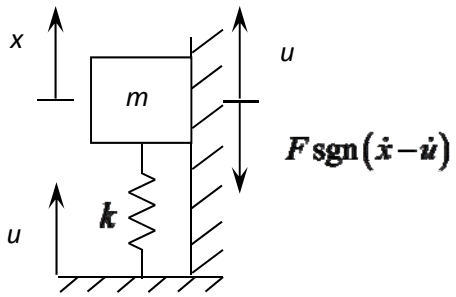

Figure 1: A one degree of freedom system isolation configuration with Coulomb friction subjected to a base input.

The equation of motion of the one degree of freedom shock isolation system with Coulomb friction for the first phase during the shock is given by:

$$m\ddot{x} + kx + Fsgn(\dot{x} - \dot{u}) = ku(t) \quad (3.1)$$

where $\omega_n = \sqrt{\frac{k}{m}}$ is the natural frequency of the system. x is the displacement of the mass and u is the displacement of the base and vertical surface shown.

A versed sine displacement shock is applied at the base to represent a shock input excitation, which closely represents real practical inputs with a smooth and continuous first two derivatives (velocity and acceleration) of the displacement. It is given by:

$$u(t) = \frac{u_{mag}}{2}\left(1 - \cos\left(\frac{2\pi t}{T_p}\right)\right) \quad [0 \le t \le T_p] \quad (3.2)$$

$$u(t) = 0 \quad [T_p \le t] \quad (3.3)$$

The shock input has duration of T_p and amplitude u_{mag}. For the analysis, the length of the versed sine base input used is chosen to be equal to natural period of the system *T*, to see whether the presence of friction can reduce the response which is large for the case of an undamped system [20]. This paper does not cover for the case of the input length much smaller and larger than the natural period of the system. The case of the input length much smaller than the natural period of the system may be worthwhile to explore in the future which typically involves high acceleration. Whilst for the case of the input length much larger than the natural period of the system the mass will closely follow the motion of the base input.

Non-dimensional parameters can be defined in terms of the physical system parameters. These are the non-dimensional displacements $y = \frac{\omega_n{}^2 x}{g}$, the non-dimensional friction force $\hat{F} = \frac{F}{mg}$, the non-dimensional base input $U = \frac{\omega_n{}^2 u}{g}$, the non-dimensional time $\tau = \omega_n t$ and differentiation with respect to non-dimensional time $y' = \frac{dy}{d\tau}$, $y'' = \frac{d^2y}{d\tau^2}$

Given these definitions, then the equations of motion can subsequently be written in non-dimensional form as

$$y'' + y + \hat{F}sgn(y' - U') = U(\tau) \quad (3.4)$$

The numerical time domain responses are solved and presented for this model and all subsequent single and two degree of freedom systems using the MATLAB Ordinary Differential Equation (ODE) solvers (e.g. ode45, ode23s). Ode45 uses a general purpose numerical Runge-Kutta integration scheme. However, in some cases, especially when friction is significant, ode23s is more efficient in solving the equations. The results were checked for accuracy and convergence for the numerical solutions for this system, as analytical solutions for this model can be obtained as it is piecewise continuous.

A single degree of freedom system with friction works well in attenuating the maximum displacement response when the length of the versed sine base input is equal to the natural period of the system, as shown in **Figures 2 (a) and 3**. However, this system experiences an acceleration discontinuity every time the direction of the friction force changes and at the start of the motion. A typical response is shown in **Figure 2(b).**

(a) (b)

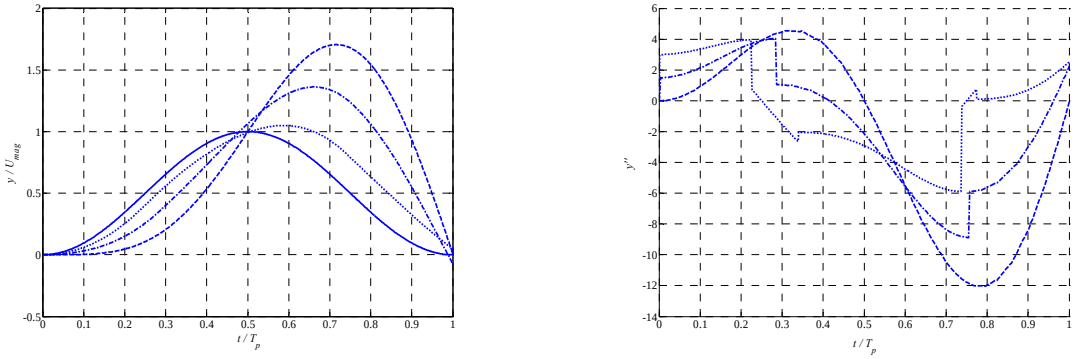

Figure 2: Response of a single degree of freedom system with friction under versed sine base input. (a) Displacement response. (b) Acceleration response. Non-dimensional base input magnitude $U_{mag} = 10$ and pulse length $T_p = T$. Solid line: base input. The dash line corresponds to $\hat{F} = 0$ ie no friction. The dash dot line $\hat{F} = 1.5$ and the dotted line: $\hat{F} = 3$.

The predicted maximum displacement response of the system as friction is varied shown in **Figure 3**. For this model, as friction increases, the maximum response is reduced until it reaches the lowest point, namely F_{opt}. In this case, the lowest maximum displacement response with respect to the base input is about 0.99 when $F_{opt} = \hat{F} = 4$ (ie $\hat{F} = 4mg$, larger than the weight of the isolated mass).

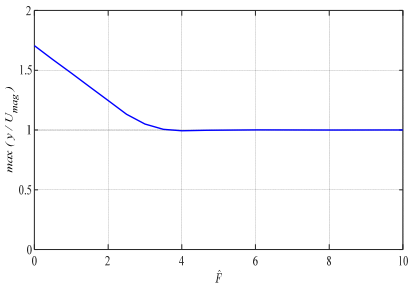

Figure 3: The maximum displacement of a single degree of freedom model under versed sine base input when the level of friction is varied. Non-dimensional base input magnitude $U_{mag} = 10$ and pulse length $T_p = T$.

Then, if the friction is further increased, the mass will stick to the friction interface and follows the displacement motion of the base instead of further displacement reduction and energy dissipation. In this case, for the friction typically greater than the value $\hat{F} = 5$, the mass moves with the same displacement as the friction surface and the base.

4. Shock response of a two degree of freedom system with friction

4.1 Displacement response

The two degree of freedom system considered in this paper is shown in **Figure 4**. It comprises of the primary structure (primary mass m_1 and stiffness k_1) and the isolated attachment (secondary mass m_2 and stiffness k_2). For this configuration, friction F is applied to the secondary mass m_2 only.

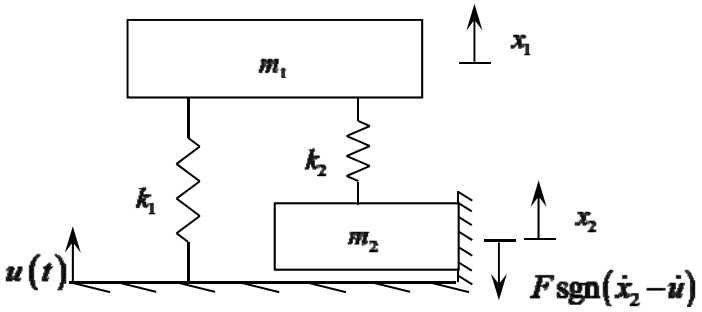

Figure 4: A two degree of freedom system isolation configuration with Coulomb friction subjected to a base input.

The two degree of freedom system that has been introduced is expected to avoid acceleration discontinuity and obtain a much smoother response at the point in time when the direction of the acting friction changes and at the start of motion, while still retaining a reduction in the displacement response of the primary isolated mass. Similar to **Section 3**, a versed sine base input is used in the calculations and the length of the base input is chosen to be equal to first natural period of the combined system defined as T_1 (calculated from eigenfrequencies of the system), to investigate whether the presence of friction can reduce the response, which is large for an undamped system. The equation of motion for the two degree of freedom shock isolation system with Coulomb friction for the first phase during the shock is given by:

$$m_1\ddot{x}_1 + k_1x_1 + k_2(x_1 - x_2) = k_1u(t) \qquad (4.1)$$

$$m_2\ddot{x}_2 - k_2(x_1 - x_2) + Fsgn(\dot{x}_2 - \dot{u}) = 0 \quad (4.2)$$

where $\omega_1 = \sqrt{\frac{k_1}{m_1}}$ and $\omega_2 = \sqrt{\frac{k_2}{m_2}}$ are the natural frequencies of the primary and secondary systems respectively when each spring is considered separately fixed at its base. x_1 and x_2 are the displacements of the two masses respectively.

Non-dimensional parameters can be defined in terms of the physical system parameters. These are the non-dimensional displacements $y_1 = \frac{\omega_1^2 x_1}{g}$ and $y_2 = \frac{\omega_2^2 x_2}{g}$, the frequency ratio $\hat{\omega} = \frac{\omega_2}{\omega_1}$, the mass ratio $\mu = \frac{m_2}{m_1}$, the stiffness ratio $\hat{k} = \frac{k_2}{k_1}$, the non-dimensional friction force $\hat{F} = \frac{F}{m_1 g}$, the non-dimensional base input $U = \frac{\omega_1^2 u}{g}$, the non-dimensional time $\tau = \omega_1 t$ and differentiation with respect to non-dimensional time $y' = \frac{dy}{d\tau}$, $y'' = \frac{d^2y}{d\tau^2}$ are as previously.

Given these definitions, then the equations of motion can subsequently be written in non-dimensional form as

$$y_1'' + y_1 + \hat{k}(y_1 - y_2) = U(\tau) \qquad (4.3)$$

$$\mu y_2'' + \hat{k}(y_2 - y_1) + \hat{F}sgn(y_2' - U') = 0 \quad (4.4)$$

Figure 5 shows the maximum displacement of the masses for different levels of friction and stiffness ratio. The results represent the response when the mass ratio is $\mu = 0.1$ i.e. m_2 is 10% of the isolated mass. For practical purposes, a small secondary mass is preferred in order to avoid a significant change in the overall weight of the system. In a later section (**Section 4.3**), the effect of the mass ratio and results for other mass ratios will be discussed. The time response plots for the two degree of freedom system are plotted in **Figure 6,** for the case of low and medium stiffness ratios with a mass ratio $\mu = 0.1$. The response for the case of a high stiffness ratio (**Figure 5(d)**) is very close to the response of a single degree of freedom system with friction, as shown in **Figures 2 and 3**.

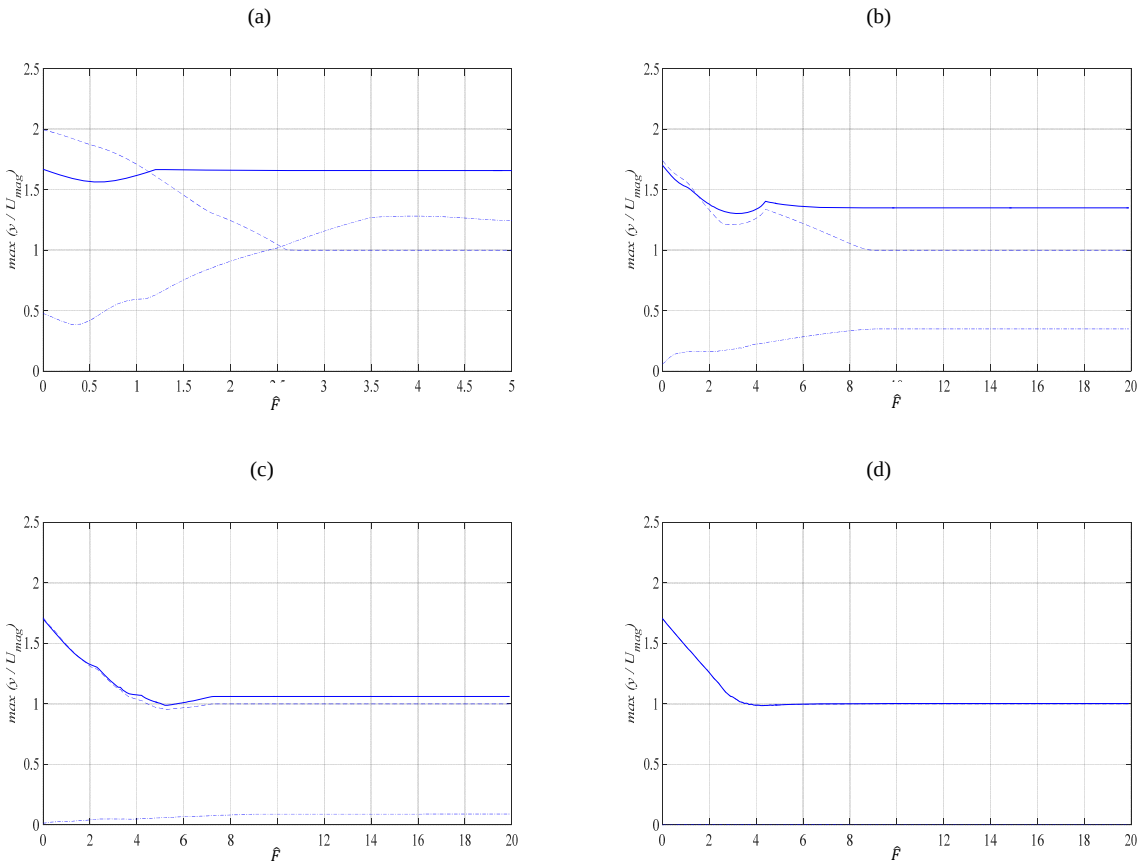

Figure 5: The maximum displacement response of the two masses in the friction system under a versed sine base input for different levels of friction. The solid line is the primary mass displacement and the dashed line is the secondary mass displacement. The dash dot line is the relative displacement, Mass ratio $\mu = 0.1$, Pulse length $T_p = T_1$, non-dimensional base input magnitude $U_{mag} = 10$, stiffness ratio $\hat{k}$. (a) $\hat{k} = 0.4$, (b) $\hat{k} = 2.5$, (c) $\hat{k} = 10$ and (d) $\hat{k} = 250$.

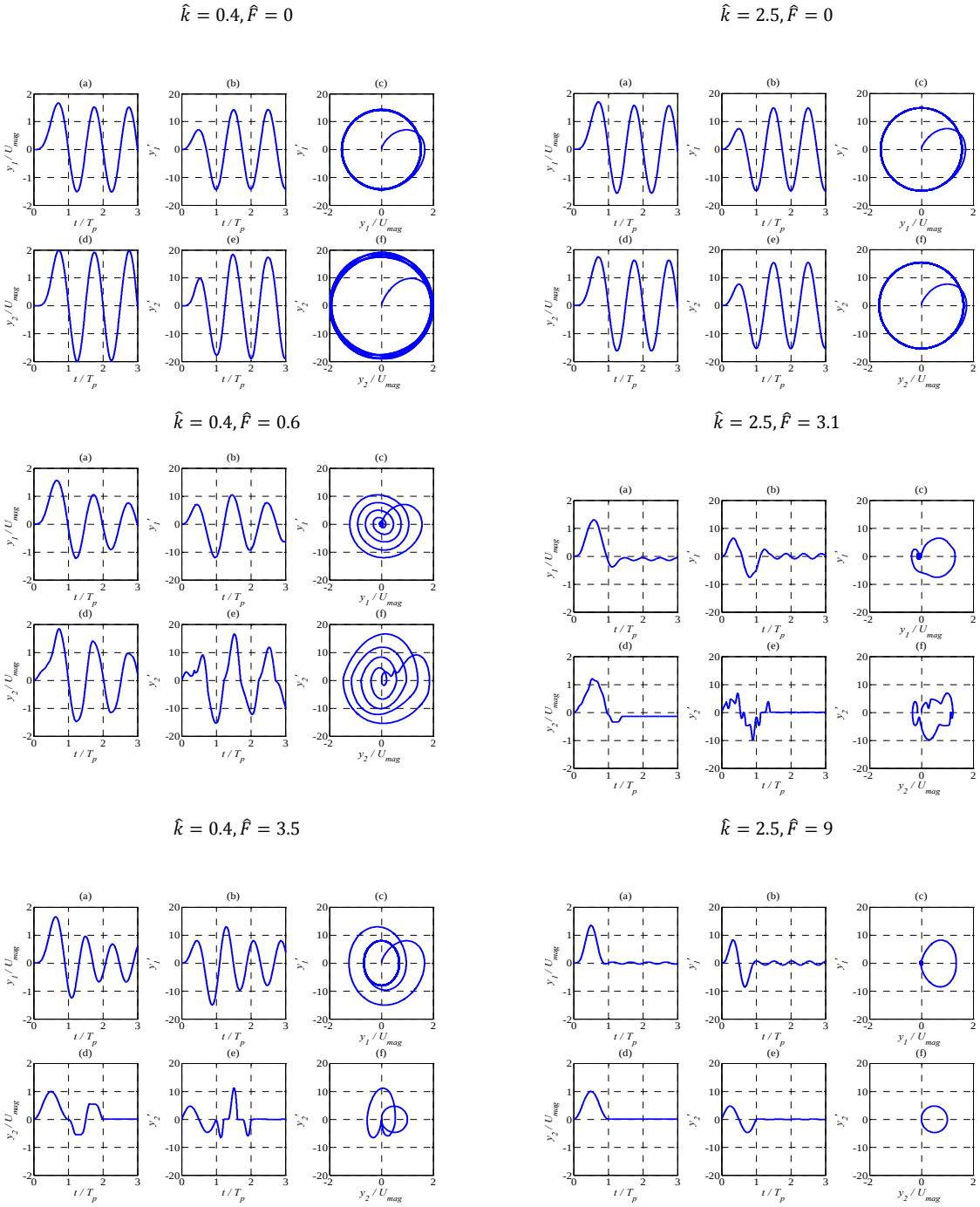

Figure 6: Time histories and phase plane plots for the case of a soft (frequency ratio $\hat{\omega} = 2$ stiffness ratio $\hat{k} = 0.4$) and a medium (frequency ratio $\hat{\omega} = 5$ stiffness ratio $\hat{k} = 2.5$) secondary spring stiffness compared to the primary spring under a versed sine base input, mass ratio $\mu = 0.1$. (a) Primary mass displacement. (b) Primary mass velocity. (c) Primary mass phase plane plot. (d) Secondary mass displacement. (e) Secondary mass velocity. (f) Secondary mass phase plane plot.

The maximum displacement of the primary mass decreases as friction increases to an upper limit which yields a maximum reduction. This is defined as $\hat{F}_{opt}$ for further reference. This is the region where the secondary mass fully slides with respect to the friction interface or experiences stick-slip motion. As the amount of friction increases, the time duration during which the secondary mass sticks onto the friction interface increases in comparison to its sliding motion. Then, when friction is further increased to be larger than $\hat{F}_{opt}$, no further reduction is obtained and the maximum displacement of the primary mass increases until the friction is large enough to cause the secondary mass to completely stop sliding on the friction interface. Above this level of friction, there is no further change to the maximum displacement of the primary mass and the primary mass becomes an undamped single degree of freedom system. The smallest maximum displacement is obtained when the secondary mass still slides on the friction interface and not when the secondary mass fully sticks on the friction interface.

For this system with a softer secondary spring one needs a lower level of friction to stick the secondary mass fully to the friction interface, compared to a system with a stiff secondary spring. For the case of $\hat{k} = 0.4$ **Figure 5a** shows that the secondary mass sticks when the non-dimensional friction is about $\hat{F} = 3.5$. However, when medium and high secondary stiffness are used as shown in **Figure 5 (b) to (d)** with $\hat{k} = 2.5$, $\hat{k} = 10$ and $\hat{k} = 250$ respectively, the secondary mass sticks when $\hat{F}$ is about 9. The system fully sticks in the cases which correspond to there being no further change in the maximum relative displacement between the masses and the maximum absolute displacement of both masses as friction is increased. The maximum relative displacement of the masses decreases as the secondary stiffness increases. This is the case when there is little compression and extension in the secondary stiffness, and both masses tend to move together with a small relative displacement.

The value of $\hat{F}_{opt}$ depends upon on the stiffness ratio. The value of $\hat{F}_{opt}$ as the stiffness ratio is varied and the normalized maximum displacement for the primary mass, $\frac{y_1}{U_{mag}}$ produced at $\hat{F}_{opt}$ are listed in **Table 1**. When the stiffness ratio is small, the reduction in the maximum displacement of the primary mass compared to an undamped system is small, for example $\frac{y_1}{U_{mag}} = 1.56$ when $\hat{k} = 0.4$. The reduction produced with respect to an undamped single degree of freedom system $\left(\frac{y_1}{U_{mag}} = 1.7\right)$ is only about 7 percent. As the stiffness ratio increases, there is a greater reduction in the maximum displacement of the primary mass and the largest reduction is produced when the stiffness ratio is $\hat{k} = 250$. For this case, $\frac{y_1}{U_{mag}}$ produced at $\hat{F}_{opt}$ is 0.99 which corresponds to a reduction of about 42 percent compared to an undamped SDOF system. This is when a two degree of freedom system behaves almost identically to a single degree of freedom system with friction applied directly to the primary mass, but there are potential reductions in the acceleration discontinuity to be discussed in the next section.

Stiffness ratio, $\hat{k}$	**Non-dimensional friction at which the smallest maximum displacement occurs, $\hat{F}_{opt}$**	**Non-dimensional primary mass displacement, $\left(\frac{y_1}{U_{mag}}\right)_{\hat{F}_{opt}}$**
0.4	0.6	1.56
2.5	3.1	1.3
10	5.3	0.99
250	4.2	0.98

Table 1: The value of friction which produces the smallest maximum displacement response of the primary mass as the stiffness ratio is varied and the corresponding displacement response. The sdof undamped system response for comparison is $\frac{y_1}{U_{mag}} = 1.7$.

4.2 Acceleration response

As stated earlier, the two degree of freedom system was introduced to avoid the instantaneous changes in the acceleration of the primary mass every time the friction force changes its direction and at the start of the motion. By applying friction to the secondary mass, a smoother or reduced acceleration discontinuities of the primary mass could be produced during the changes in the direction of the friction force and at the start of the motion.

The acceleration response of the primary mass for different stiffness ratios is plotted in **Figure 7**. This is based on the friction value equal to $\hat{F}_{opt}$, which is known to produce the smallest maximum displacement for the primary mass at each stiffness ratio. Therefore, it is beneficial to see whether this friction value also could produce a good acceleration response for the primary mass.

(a) (b)

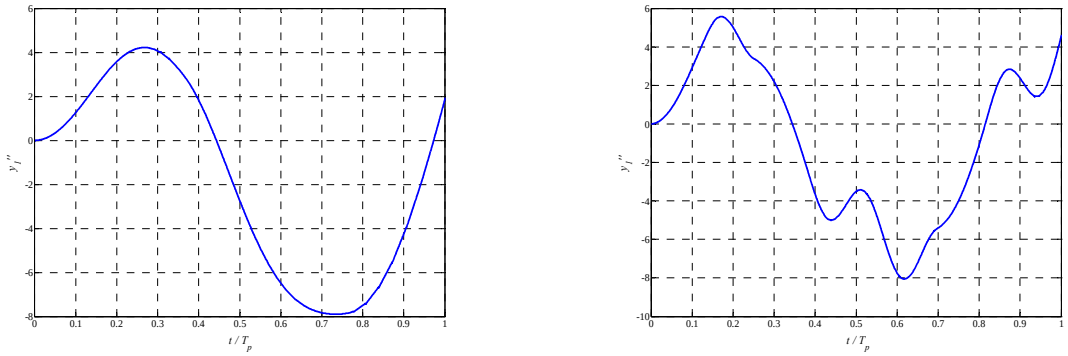

(c)

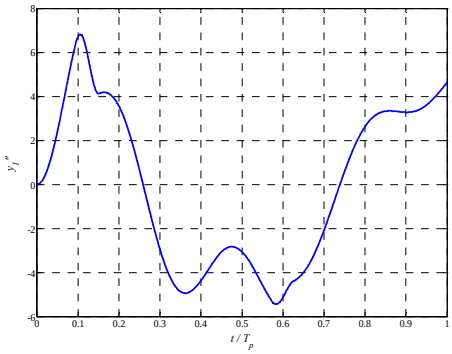

Figure 7: Acceleration response of the primary mass of the two degree of freedom model under a versed sine base input when $\hat{F} = \hat{F}_{opt}$. (a) stiffness ratio $\hat{k} = 0.4$, $\hat{F}_{opt} = 0.6$. (b) stiffness ratio $\hat{k} = 2.5$, $\hat{F}_{opt} = 3.1$. (c) stiffness ratio $\hat{k} = 10$, $\hat{F}_{opt} = 5.3$.

From **Figure 7**, one can observe that the acceleration of the primary mass is smooth when the stiffness ratio is small. As the stiffness ratio is increased, the acceleration of the primary mass changes more sharply every time the friction force changes its directions and at the start of the motion. This is because of a stronger coupling and higher forces acting between the primary and secondary masses on which the friction is applied. However, for all of these cases shown, the primary system acceleration response is improved and smoother than the case of a single degree of freedom system with friction (see **Figure 2(b)** for comparison).

4.3 Effect of the mass ratio on the shock response

For practicality, a small secondary mass is preferred. In the previous sections, a small secondary mass was used which is ten times smaller than the primary mass. In this section, variations in the secondary mass are investigated to see whether increasing the secondary mass could give a smaller maximum displacement of the primary mass during the shock. Two mass ratio values were chosen, which are $\mu = 0.32$ and $\mu = 1$ which will be compared with $\mu = 0.1$. The maximum displacement of the primary mass as friction is varied for these mass ratio values can also be seen in **Figure 8**. The dash lines in the plot correspond to the case of the mass ratio $\mu = 0.32$ and the dash dot lines correspond to the case of the mass ratio $\mu = 1$. This is compared with the solid line for the mass ratio $\mu = 0.1$. The time response plots for the corresponding cases are plotted in **Figures 9 and 10** respectively.

There is a large difference in the maximum displacement response of the primary mass for a different mass ratio only when the stiffness ratio is small (**Figure 8 (a)**). As the stiffness ratio increases, the influence of the mass ratio on the behaviour of the system becomes less significant; hence reduction in the difference in the maximum displacement response (**Figure 5 (b) to (d)**). The large difference that occurs when the stiffness ratio is small is caused by the existence of two significant modes that influence the response of the system. The first mode is where the two masses move together in phase and the second mode is the mode where the second mass moves in the opposite direction compared to the first mass. As the mass ratio is varied for a fixed stiffness ratio, the frequency ratio $\hat{\omega} = \frac{\omega_2}{\omega_1}$ changes. For a small stiffness ratio, the change in the frequency ratio produces a large change in the displacement response of the masses because it affects how the two modes interact and combine to produce the overall response of the system. When the stiffness ratio is larger, the second mode where masses move out of phase, shifts to a higher frequency and its contribution to the response of the system is quite small. In this case, only one mode (in phase mode) dominates the response of the system and a small difference is produced in the response of the two masses.

For the case of a medium value for the stiffness ratio, $\hat{k} = 2.5$ and $\hat{k} = 10$, the difference caused by a variation in the mass ratio can only be seen for high levels of friction. For high friction, the maximum displacement response of the primary mass is smaller for the case of the larger mass ratio. This is because, the primary mass oscillates at a lower amplitude when the secondary mass fully sticks for high friction and when the secondary mass (mass ratio) is large. As the stiffness ratio increases to a higher value, this difference becomes less significant.

Another effect due to the variation in the mass ratio is the change in the value of friction that causes the secondary mass to fully stick on the friction interface. For a larger mass ratio, less friction is needed to cause the secondary mass to fully stick. For example, in the case of a small stiffness ratio ($\hat{k} = 0.4$), the secondary mass fully sticks at $\hat{F} = 2.1$ when the mass ratio $\mu = 1$, at $\hat{F} = 2.3$ when the mass ratio $\mu = 0.32$ and $\hat{F} = 3.5$ when the mass ratio $\mu = 0.1$. This is because, lower friction is sufficient to cause the large secondary mass to stop sliding relative to the friction interface. This also applies to the case for other stiffness ratios ($\hat{k} = 2.5$, $\hat{k} = 10$ and $\hat{k} = 250$), although it becomes less significant at higher stiffness ratios.

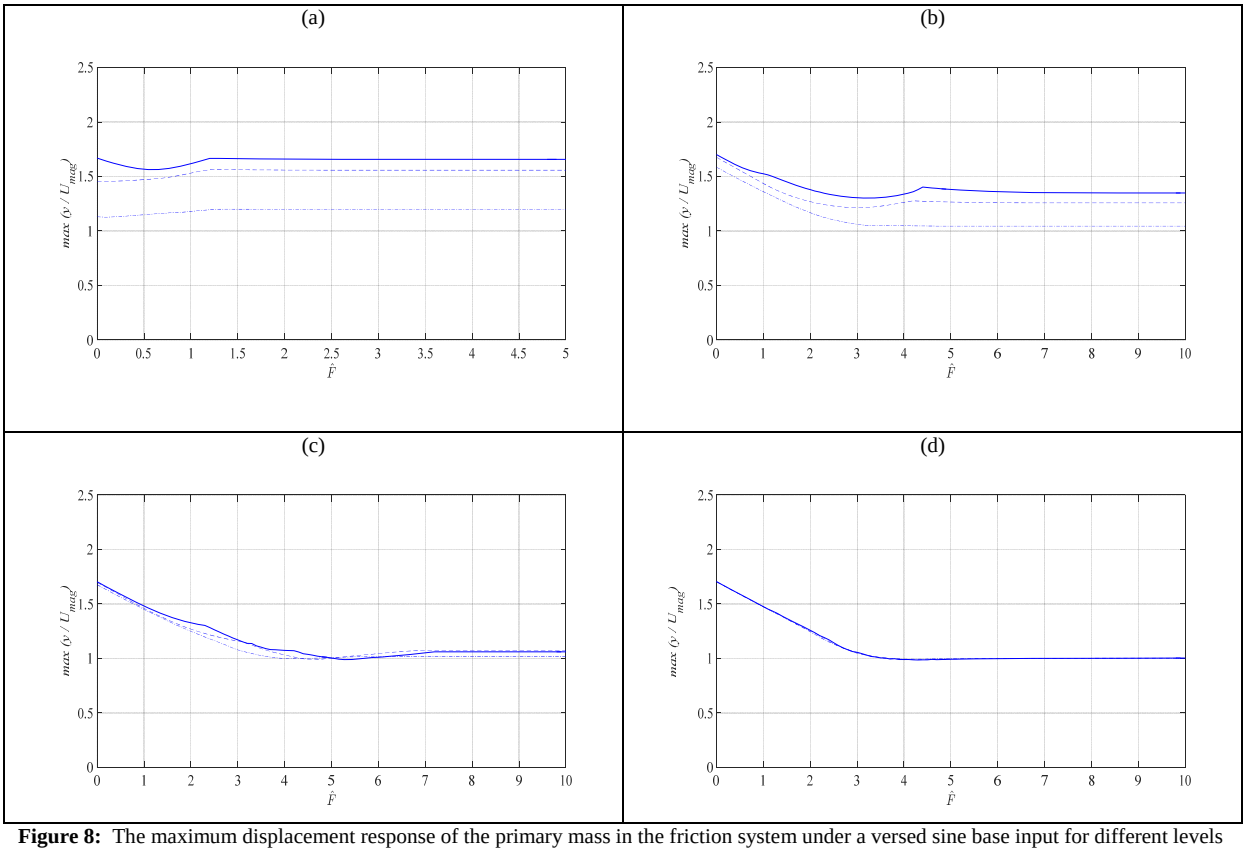

Figure 8: The maximum displacement response of the primary mass in the friction system under a versed sine base input for different levels of friction. Stiffness ratio $\hat{k}$: (a) $\hat{k} = 0.4$, (b) $\hat{k} = 2.5$, (c) $\hat{k} = 10$,(d) $\hat{k} = 250$. Mass ratio $\mu = 0.1$ (solid line), Mass ratio $\mu = 0.32$ (dash line), Mass ratio $\mu = 1$ (dash dot line). Pulse length $T_p = T_1$, non-dimensional base input magnitude $U_{mag} = 10$.

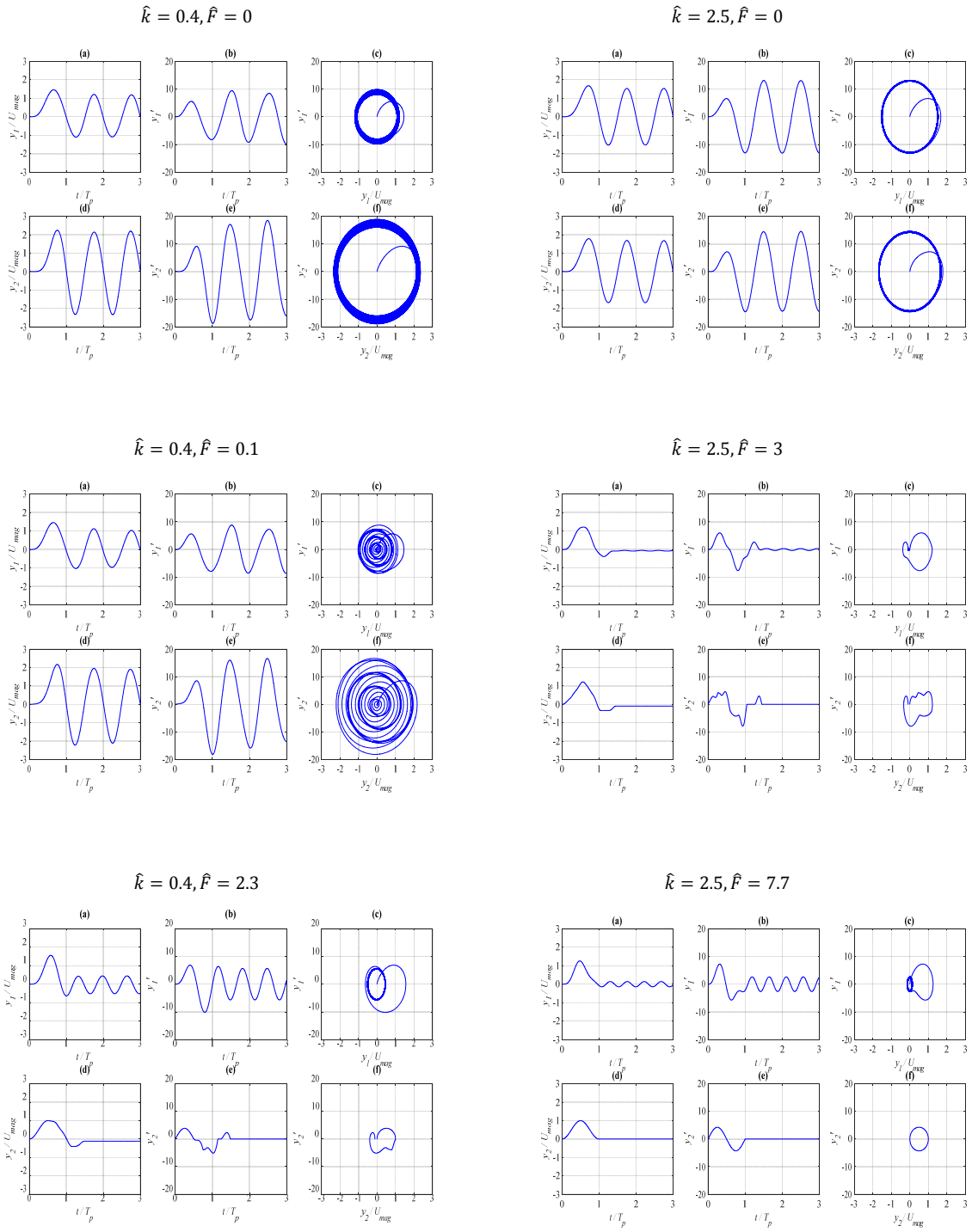

Figure 9: Time histories and phase plane plots for the case of a soft (frequency ratio $\hat{\omega} = 1.12$, stiffness ratio $\hat{k} = 0.4$) and a medium (frequency ratio $\hat{\omega} = 2.8$, stiffness ratio $\hat{k} = 2.5$) secondary spring stiffness compared to the primary spring under a versed sine base input, mass ratio $\mu = 0.32$. (a) Primary mass displacement. (b) Primary mass velocity. (c) Primary mass phase plane plot. (d) Secondary mass displacement. (e) Secondary mass velocity. (f) Secondary mass phase plane plot.

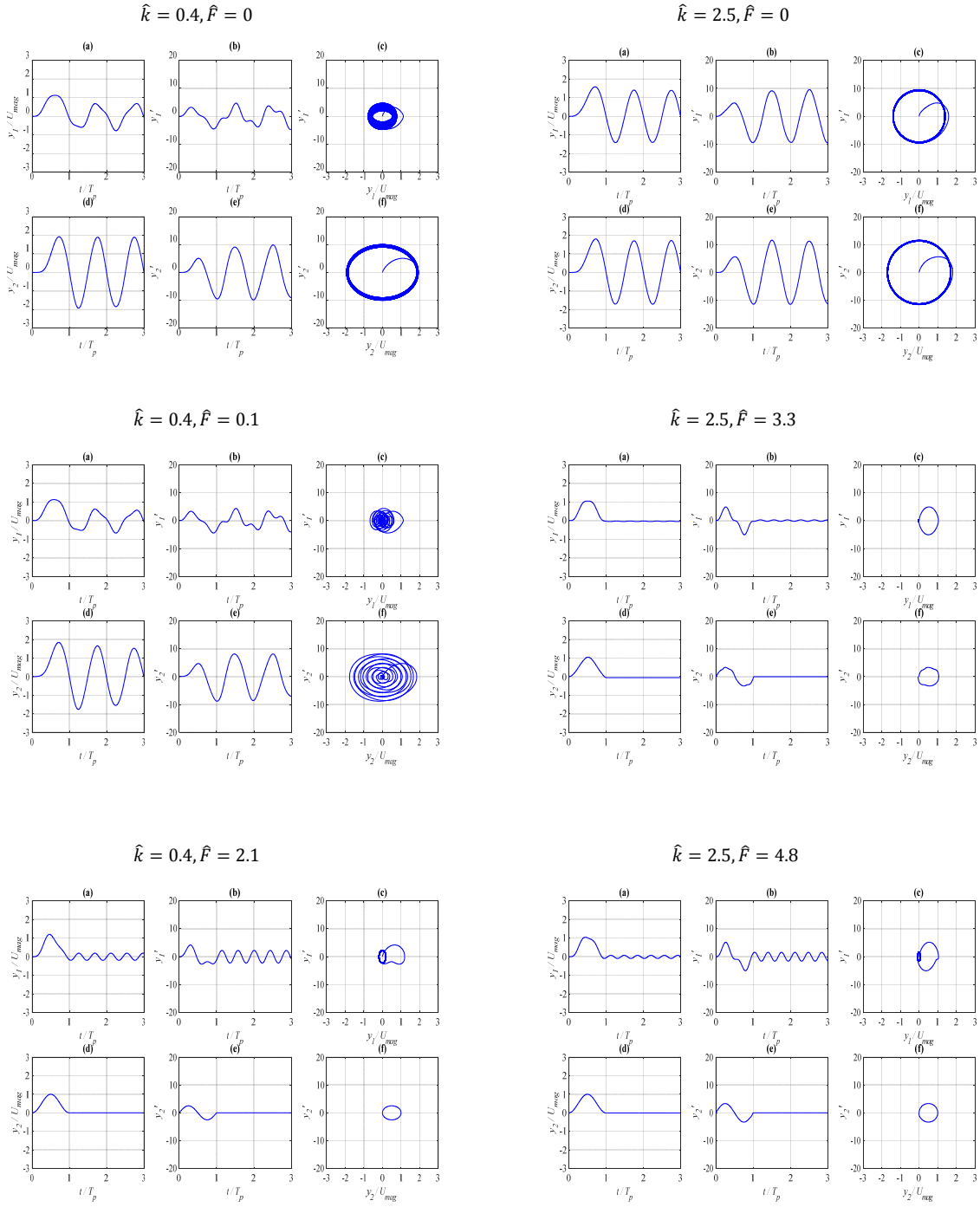

Figure 10: Time histories and phase plane plots for the case of a soft (frequency ratio $\hat{\omega} = 0.63$, stiffness ratio $\hat{k} = 0.4$) and a medium (frequency ratio $\hat{\omega} = 1.58$, stiffness ratio $\hat{k} = 2.5$) secondary spring stiffness compared to the primary spring under a versed sine base input, mass ratio $\mu = 1$. (a) Primary mass displacement. (b) Primary mass velocity.(c) Primary mass phase plane plot. (d) Secondary mass displacement. (e) Secondary mass velocity. (f) Secondary mass phase plane plot.

5. Design and Experimental Validation

A series of experiments were performed to validate the response of a two degree of freedom system with friction. The experiments were conducted in a few stages as shown in **Figure 11**. The stages will be discussed in detail in the following sections.

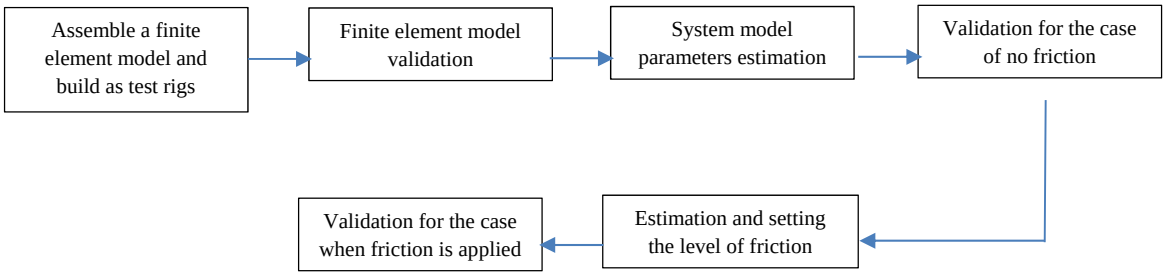

Figure 11: Experimental design and validation steps

5.1 Assemble a finite element model and build as test rigs

The experimental setup designed is a T beam comprising two aluminium beams, namely a primary (150×15×3.3 mm) and a secondary beam as shown in **Figure 12** which are connected with a bolted connection. Two different secondary beams were used, a thin (160×15×0.9 mm) and thick secondary beam (160×15×3 mm). This is to compare between the response of a single and two degree of freedom system. It is expected that the configuration with a thin secondary beam vibrates in two dominant modes at low frequencies and behaves like a two degree of freedom system. On the other hand, it is expected that the configuration with a thick secondary beam behaves like a single degree of freedom system with one dominant mode at low frequencies.

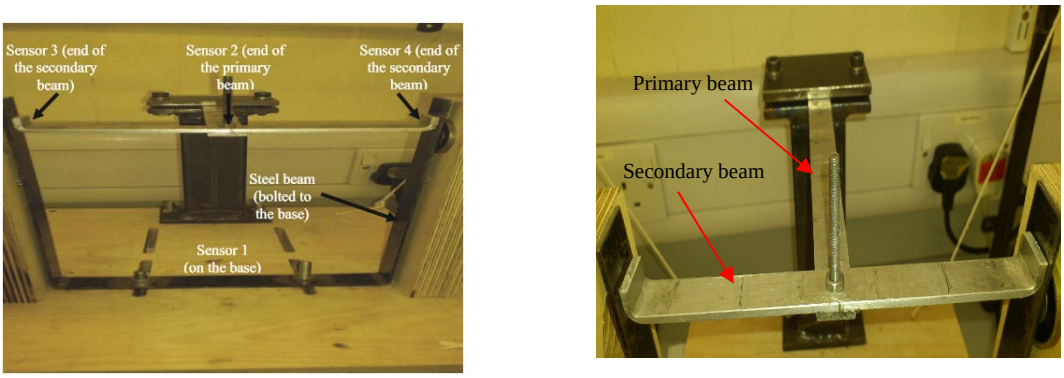

Figure 12: Test rig built for experimental validation

A finite element model was assembled in ANSYS to predict the first few modes of the beam system and verify whether it can be used to represent a single or two degree of freedom system in the low frequency range. In the model, one end of the primary beam was set as a fix end and another end to be a free end on which the middle of the secondary beam was attached. From the finite element model, the system with the thin secondary beam has three natural frequencies below 120 Hz. There are two coupled modes, which were identified as a flexural mode of the primary beam predicted at 59.4 Hz and a flexural mode of the secondary beam predicted at 112.9 Hz. There is also another mode between these two modes, which was identified as a torsional mode of the primary beam at 80.5 Hz. However, the torsional mode is not significant in comparison with the flexural modes, which was determined from the next step in the experiment. This will be discussed further in Section 5.3. Therefore, only two modes dominate the response of the system for the frequency range up to 120 Hz and closely represent a two degree of freedom system behaviour. For the system with the thick secondary beam, the torsional mode of the primary beam and the flexural mode of the secondary beam increases significantly to 106.1 and 430.9 Hz respectively. The flexural mode of the primary beam, however reduced to around 48.8 Hz. This closely represents a single degree of freedom system in the low frequency range. The predicted mode shapes of the first three modes of the T beam system for the case of thin and thick secondary beams are shown in **Figure 13** and **Figure 14** respectively.

59.4 Hz | 80.5 Hz | 112.9 Hz

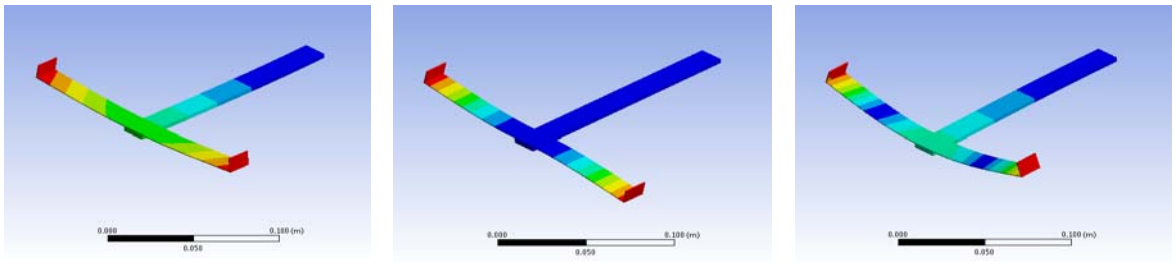

Figure 13: Predicted Mode shapes of the T beam system with thin secondary beam

48.8 Hz | 106.1 Hz | 430.9 Hz

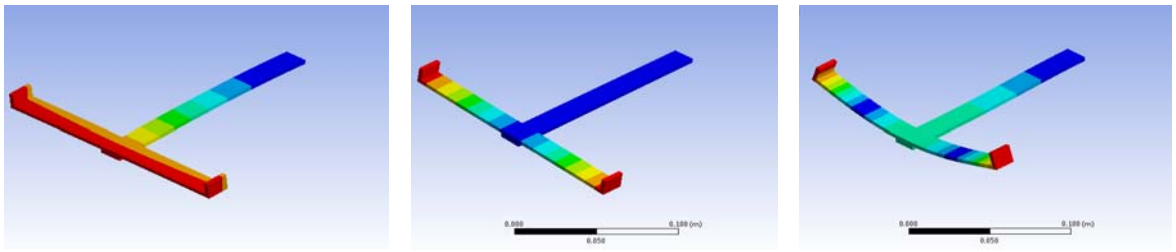

Figure 14: Predicted Mode shapes of the T beam system with thick secondary beam

A steel beam was used to apply friction to the ends of the secondary beam. The steel beam was bolted to the base, so that the friction interface could move with the base input following the model. There is a small screw at each end of the secondary beam for the purpose of adjusting the normal force between the ends of the secondary beam and the steel beam. The experimental rig was hung with four cords and a shaker (Derritron VP4) was attached below the base to apply a base input to the rig.

5.2 Finite element model validation

A scanning laser vibrometer (Polytec PSV 400) was used to measure the response and verify the first three modes predicted by the finite element model analysis. For this case, only the system with thin secondary beam was used which potentially represents a two degree of freedom system at low frequencies. Broadband random excitation from the vibrometer was used to drive the shaker and the results were compared with the finite element model.

Table 2 shows the comparison between the finite element model prediction and measured natural frequencies for the first three modes of the T beam system for the case of the thin secondary beam. The results are within 6.9% difference.

Modes	Finite element predicted natural frequency (Hz)	Measured natural frequency (Hz)	Percentage difference
First mode (flexural mode of the primary beam)	59.4	58.0	2.4
Second mode (torsional mode of the primary beam)	80.5	75.3	6.9
Third mode (flexural mode of the secondary beam)	112.9	111.8	0.98

Table 2: Comparison between finite element predicted and measured natural frequencies.

Figure 15 shows the first three measured operational deflection shape (ODS) of the T beam system. In order to verify the correlation between the finite element modal and measured results, the Modal Assurance Criterion [23] was used. It is a widely used technique to estimate the degree of correlation between mode shape vectors [24]. Eleven measurement points and three modes were used for this calculation using **Equation 5.1**.

58.0 Hz 75.3 Hz 111.8 Hz

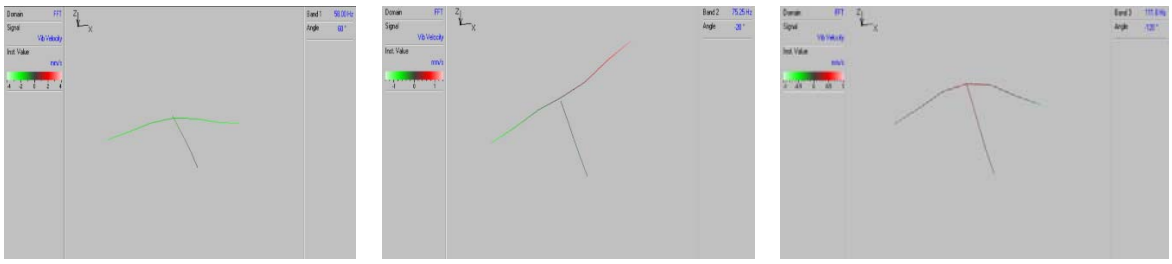

Figure 15: Operational deflection shapes of the T beam system with thin secondary beam

$$MAC(i,j) = \frac{\left|\{\Phi_{measured}\}_i^T \{\Phi_{FE}\}_j\right|^2}{\left|\{\Phi_{measured}\}_i^T \{\Phi_{measured}\}_i\right| \cdot \left|\{\Phi_{FE}\}_j^T \{\Phi_{FE}\}_j\right|} \quad (5.1)$$

From the results, predicted mode shapes from finite element model are within 3 percent difference with their measured operating deflection shape. The lowest MAC value between the predicted modes and measured deflection shapes are 0.97.

5.3 System model parameters estimation

Consider a two degree of freedom model as shown in **Figure 16** to represent the T beam system behaviour with a thin secondary beam at low frequencies. The next experiment was performed to measure the acceleration transmissibility of the beam system and fit the measured data to the two degree of freedom model equations (**Equation 5.2** and **Equation 5.3**). The experiment was only performed with the thin secondary beam to estimate the physical parameters of the two degree of freedom system namely the stiffness (k_1 and k_2), structural damping (η_1 and η_2) and mass (m_1 and m_2). In this section, friction was set to zero.

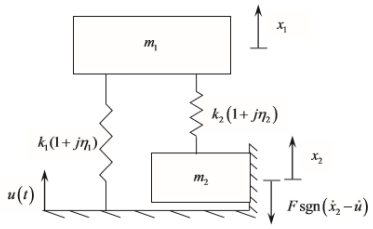

Figure 16: Two degree of freedom model for comparison with T beam response

The acceleration transmissibilities without friction for the model shown in **Figure 16** are

$$\frac{\ddot{x}_1}{\ddot{u}} = \frac{\left(k_1(1+j\eta_1)\right)\left(k_2(1+j\eta_2)-m_2\omega^2\right)}{\left(k_1(1+j\eta_1)+k_2(1+j\eta_2)-m_1\omega^2\right)\left(k_2(1+j\eta_2)-m_2\omega^2\right)-k_2{}^2(1+j\eta_2)-jk_2{}^2\eta_2(1+j\eta_2)} \quad (5.2)$$

$$\frac{\ddot{x}_2}{\ddot{u}} = \frac{k_2(1+j\eta_2)}{\left(k_2(1+j\eta_2)-m_2\omega^2\right)}\left(\frac{\ddot{x}_1}{\ddot{u}}\right) \quad (5.3)$$

In the experiment, four accelerometers were used to record the data, one at the base of the rig, one at the end of the primary beam and two at opposite ends of the secondary beam. Two accelerometers were used for the secondary beam to confirm that no significant difference in the response and the level of friction applied at each end of the secondary beam in the later experiment. The response at the end of the primary beam was compared with the response of the primary mass and the response at the end of the secondary beam was compared with the response of the secondary mass in the theoretical model. The accelerometers are connected to an analyser and a computer for processing and calculating the frequency response functions (acceleration transmissibility) based on the acceleration signals. The acceleration transmissibility calculated were between the base and both the primary and secondary beam.

Figure 17 shows the measured acceleration transmissibility of the T beam at low frequencies between 0 to 130 Hz. From the figure, two frequencies are dominant, in the region of 55 Hz and 108 Hz corresponding to the flexural modes of the primary beam and

secondary beam respectively. There is another mode between these two frequencies, around 75 to 80 Hz, corresponding to a torsional mode of the primary beam which has been predicted by finite element model in **Section 5.1**. However, the response was small in comparison with modes at other two frequencies and can be considered negligible.

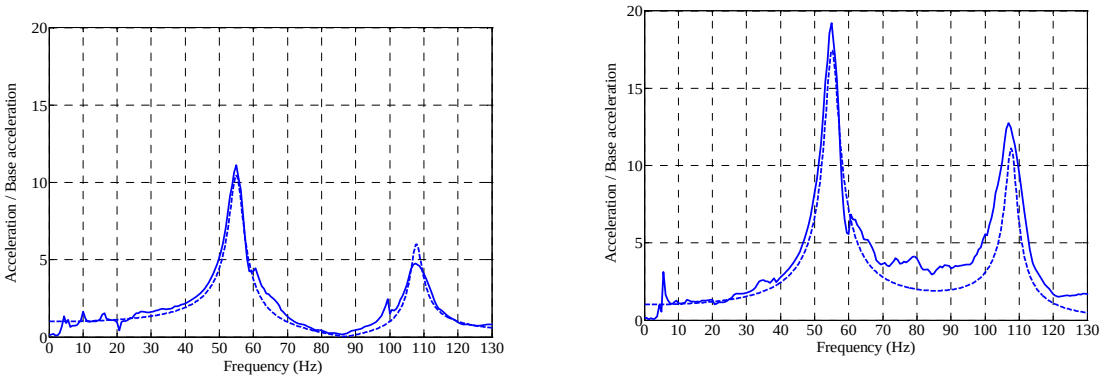

Figure 17: The measured acceleration transmissibility measured from the experiment for the case of no friction and thin secondary beam. (a) The primary system response. Solid line: Acceleration at the end of the first beam (sensor 2). Dash line: Predicted acceleration of the primary mass using fitted parameters. (b) The secondary system response. Solid line: Acceleration at the end of the secondary beam (sensor 3). Dashed line: Predicted acceleration of the secondary mass using fitted parameters.

A MATLAB fitting function was utilised to search for a combination of second degree of freedom parameters that fit the acceleration transmissibility obtained from the measurements. The least square error fit between the measured and model transmissibility was calculated (**Equation 5.4**) such that the summation over the frequency range of the available data is minimised.

$$\sum \left| \left(\mathrm{Re}\left(\frac{\ddot{x}_1}{\ddot{u}}\right)_{measured} - \mathrm{Re}\left(\frac{\ddot{x}_1}{\ddot{u}}\right)_{model} \right)^2 + \left(\mathrm{Re}\left(\frac{\ddot{x}_2}{\ddot{u}}\right)_{measured} - \mathrm{Re}\left(\frac{\ddot{x}_2}{\ddot{u}}\right)_{model} \right)^2 + \left(\mathrm{Im}\left(\frac{\ddot{x}_1}{\ddot{u}}\right)_{measured} - \mathrm{Im}\left(\frac{\ddot{x}_1}{\ddot{u}}\right)_{model} \right)^2 + \left(\mathrm{Im}\left(\frac{\ddot{x}_2}{\ddot{u}}\right)_{measured} - \mathrm{Im}\left(\frac{\ddot{x}_2}{\ddot{u}}\right)_{model} \right)^2 \right| \quad (5.4)$$

The estimated model parameters are given in the **Table 3**. The acceleration transmissibilities based on the estimated model parameters are plotted on the same figure as the measured acceleration transmissibilities (**Figure 17**) for comparison. They are in very close agreement with each other. The corresponding estimates of the modal damping from the measured response are equal to 0.08 (fundamental mode around 55 Hz) and 0.06 for the second mode (around 107 Hz).

Parameters	Estimated values
k_1	4350.5 N/m
k_2	2279.1 N/m
m_1	0.024 kg
m_2	0.008 kg
η_1	0.09
η_2	0.02
Stiffness ratio, $\hat{k} = \frac{k_2}{k_1}$	0.52
Mass ratio, $\mu = \frac{m_2}{m_1}$	0.32
First natural frequency of a coupled system, ω_1	429.1 rad/s
Frequency ratio, $\hat{\omega} = \frac{\omega_2}{\omega_1}$	1.27

Table 3: Two degree of freedom model system parameters estimated by fitting the two degree of freedom model equations with the measured data from the experiment.

For the system with the thick secondary beam, the measured acceleration transmissibility is dominated by the first mode (flexural mode of the primary beam) at 45 Hz, while at a very low amplitude was observed the torsional mode of the primary beam and the flexural mode of the secondary beam, as shown in **Figure 18**. Both of the low amplitude modes also shifted to a higher frequency as predicted.

In this case, the T beam system closely follow the behaviour of a single degree of freedom system below 100 Hz with dominant frequency of 45 Hz.

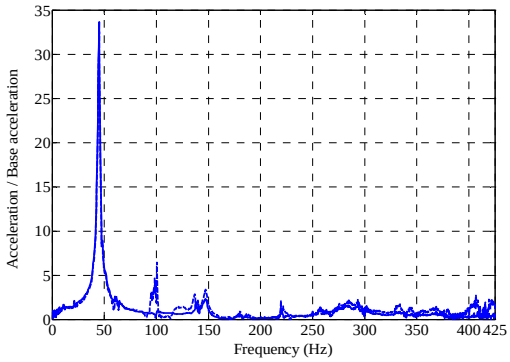

Figure 18: The acceleration transmissibility measured from the experiment for the case of no friction and a thick secondary beam. Solid line: Acceleration at the end of the first beam (sensor 2). Dash line: Acceleration at the end of the secondary beam (sensor 3).

5.4 Validation for the case of no friction

For the shock input application, a versed sine base input was generated using MATLAB and exported as a waveform audio format (WAV) file. The file can be played through a PC sound card to drive an electrodynamic shaker via an amplifier. This technique was used by Ramirez [25] to apply a versed sine base input with minimum residual vibration. It is preferred to have a base input with as small a residual response as possible to closely represent a theoretical versed sine.

Before conducting experiment with friction, it is important to perform a validation for the case of no friction to verify that the system behaves as predicted by theoretical model when the shock input is applied. The measured acceleration was filtered with a high pass filter and subsequently integrated to obtain velocity. Subsequently, the velocity is filtered again and integrated to obtain displacement. The low frequencies were filtered to avoid output drift. The displacement of both the T beam and two degree of freedom model are normalised with respect to the maximum base input displacement. The time axis is normalised with respect to the length of the pulse, about 0.02 s, which is in the region of the first natural period of the T beam system (0.018 s).

Figure 19 shows the measured and simulated normalised displacement response of the T beam system with the thin secondary beam and no friction. It was observed that the versed sine base input produced was not a perfectly symmetric. It follows closely the theoretical versed sine base input up to half of the pulse length. Then, it started to drift away slightly from the theoretical curve. This explains the slight difference between the measured response and simulation after half of the pulse length.

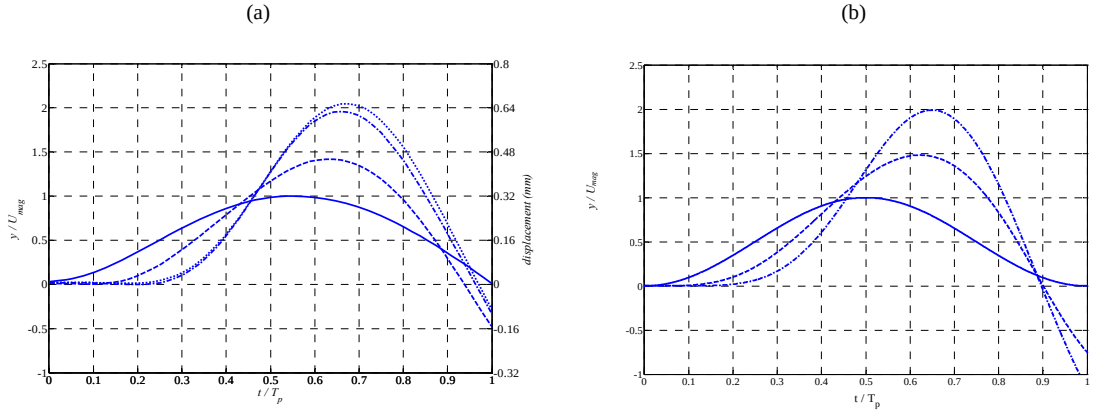

Figure 19: Measured displacement response of the thin secondary beam system with no friction and its comparison with simulation. (a) Measured. Solid line: Base input. Dash line: Response at the end of the primary beam (sensor 2). Dash dot line: Response at the end of the secondary beam (sensor 3). Dot line: Response at the end of the secondary beam (sensor 4). (b) ODE simulation. Solid line: Base input. Dash line: Response of the primary mass. Dash dot line: Response at the secondary mass.

Figure 20 shows the measured and simulated normalised displacement response of the T beam system with the thick secondary beam and no friction. Similar to the case with the thin beam, the difference between measured and simulation displacement response is caused by slight deviation of the experimental base input compared to the theoretical versed sine curve. For example, from normalised time up to 0.75 of the fundamental system period, the simulation response is larger than the measured response because the theoretical versed sine base input is larger than the actual experimental base input. Then, after half of the pulse length, the experimental base input becomes larger than the theoretical versed sine base input which caused the simulation response to reduce and become smaller than the measured response.

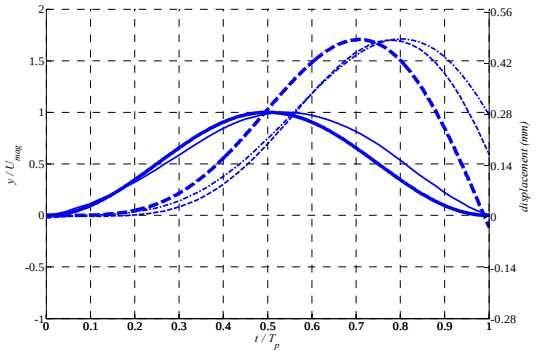

Figure 20: Displacement response of the thick secondary beam system with no friction. Thick solid line: Simulation base input. Thick dash line: Response of a single degree of freedom system. Thin solid line: Experimental base input. Thin dash line: Response at the end of the primary beam. Thin dash dot line: Response at the end of the secondary beam.

5.5 Estimation and setting the level of friction (free vibration)

As described in **Section 5.1**, the normal force and hence friction is adjusted by a small screw at each end of the secondary beam. The normal force was set at certain level to give different levels of friction. In order to estimate the value of friction after it was set, a free vibration test was performed on the T beam system. The friction value can be estimated by fitting the results from the free vibration test with the analytical solution for any cycle of vibration that minimises the least square error. This applies only for the case when friction is not too large to cause the secondary mass to stick (within the sliding region). Several cycles from the experimental data were used to ensure the level of friction is nearly constant, unchanged and repeatable. The value of friction from the experiment was subsequently used to perform simulations for the shock response of the system with friction. The predicted results will be compared with the subsequent experiment for shock application, which will be discussed in the next section.

The equations of motion 4.1 and 4.2 with no base motion, $u = \dot{u} = 0$, can be transformed into equations of motion in the two distinct modes depending on the sign of the secondary mass velocity $\dot{x}_2$. Initially, the displacement of the primary and secondary mass can be split into two modal equations with the solution of u_1 and u_2 for displacement in each mode respectively as shown in **Equation 5.5**.

$$\begin{pmatrix} x_1 \\ x_2 \end{pmatrix} = \begin{pmatrix} \Phi_{11} & \Phi_{12} \\ \Phi_{21} & \Phi_{22} \end{pmatrix} \begin{pmatrix} u_1 \\ u_2 \end{pmatrix} \qquad (5.5)$$

$\Phi = \begin{pmatrix} \Phi_{11} & \Phi_{12} \\ \Phi_{21} & \Phi_{22} \end{pmatrix}$ is the mode shape matrix whose columns represent the undamped modes.

The solution has to be evaluated segment by segment based on the sign of the secondary mass velocity and initial condition of the different segments. Hence, when $\dot{x}_2$ positive, **equation 5.6** is used and when $\dot{x}_2$ is negative, **equation 5.7** is used.

$$\begin{aligned} \ddot{u}_1 + \omega_1^2 u_1 + \Phi_{21} F = 0 \\ \ddot{u}_2 + \omega_2^2 u_2 + \Phi_{22} F = 0 \end{aligned} \qquad (5.6)$$

$$\begin{aligned} \ddot{u}_1 + \omega_1^2 u_1 - \Phi_{21} F = 0 \\ \ddot{u}_2 + \omega_2^2 u_2 - \Phi_{22} F = 0 \end{aligned} \qquad (5.7)$$

$\omega_n = \begin{pmatrix} \omega_1 & 0 \\ 0 & \omega_2 \end{pmatrix}$ is the natural frequency matrix of the two degree of freedom system. The analytical solution for both equations can be computed as **equation 5.8** and **5.9** respectively; for each piecewise linear response.

$$u_1(t) = A_1 \cos \omega_1 t + B_1 \sin \omega_1 t - \frac{\Phi_{21} F}{\omega_1^2}$$
$$u_2(t) = A_2 \cos \omega_2 t + B_2 \sin \omega_2 t - \frac{\Phi_{22} F}{\omega_2^2} \quad (5.8)$$

$$u_1(t) = A_1 \cos \omega_1 t + B_1 \sin \omega_1 t + \frac{\Phi_{21} F}{\omega_1^2}$$
$$u_2(t) = A_2 \cos \omega_2 t + B_2 \sin \omega_2 t + \frac{\Phi_{22} F}{\omega_2^2} \quad (5.9)$$

The coefficients A_1, A_2, B_1 and B_2 can be calculated by using the initial conditions for each segment.

If $\dot{x}_2$ is positive,

$$u_1(0) = A_1 - \frac{\Phi_{21} F}{\omega_1^2}$$
$$u_2(0) = A_2 - \frac{\Phi_{22} F}{\omega_2^2}$$
$$\dot{u}_1(0) = B_1 \omega_1$$
$$\dot{u}_2(0) = B_2 \omega_2$$

If $\dot{x}_2$ is negative,

$$u_1(0) = A_1 + \frac{\Phi_{21} F}{\omega_1^2}$$
$$u_2(0) = A_2 + \frac{\Phi_{22} F}{\omega_2^2}$$
$$\dot{u}_1(0) = B_1 \omega_1$$
$$\dot{u}_2(0) = B_2 \omega_2$$

The initial conditions for every segment were based on the final condition of the previous phase of the motion.

Depending on the sign of $\dot{x}_2$ and the initial conditions, the correct analytical solution can be calculated as the motion progresses and can be fitted into the MATLAB fitting functions to estimate the value of friction. The value of friction was checked so that no significant change throughout the motion (relatively constant) to ensure the value used for simulation to predict and validate the result of the shock application is correct. The estimated friction will be used in the next section with the estimated two degree of freedom model parameters calculated from the previous section, to validate the time response of the system with Coulomb friction subjected to a versed sine base input. However, it is still expected there is slight variation in the friction values since friction is most likely changing as the beam moves, as a result of friction surface changes, and the bending of the steel beam friction interface. This may influence and create differences between the friction applied to end of the secondary beam. **Figure 21** shows some examples of comparison between the free vibration experimental results and the analytical solution using the friction estimated from the fitting process. The friction values estimated from the fitting process are next to the figure. As expected, there is variation in the estimated friction values,which is about ±20% relative to 0.5. All of the estimated values for non-dimensional friction $\hat{F}$ are between 0 and 1, which is still in the sliding region. From the simulations, it is predicted the secondary mass will fully stick when the non-dimensional friction $\hat{F}$ is about equal to 1.

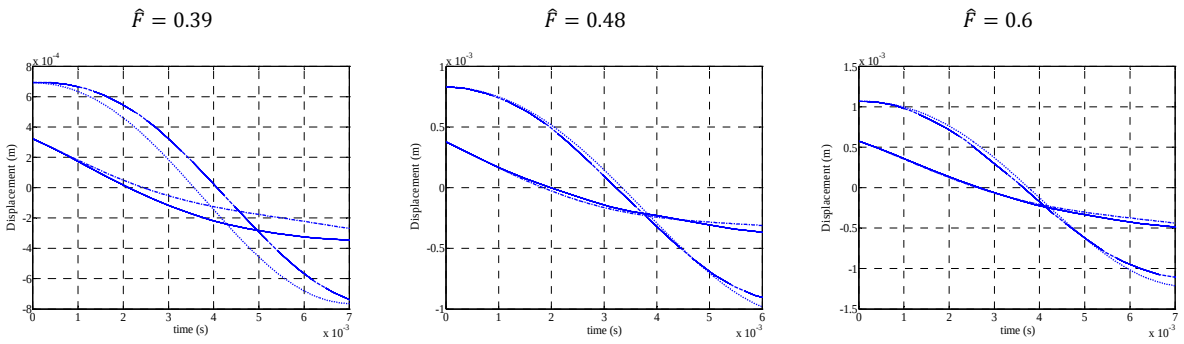

Figure 21: Comparison of the free vibration response of the beam system with the analytical solutions to estimate the value of friction. Solid line: Response at the end of the primary beam (sensor 2). Dash line: Response at the end of the secondary beam (sensor 3). Dash dot line: Free vibration response of the primary mass response with friction estimated. Dot line: Free vibration response of the secondary mass response with friction estimated.

5.6 Validation for the case when friction is applied (Thin secondary beam with friction : under base excitation)

In this case, two levels of friction were applied to the system with thin secondary beam, namely intermediate and high friction. When intermediate friction is applied, it is expected that the end of the secondary beam slides with respect to the friction interface and when high friction is applied, it is expected that the end of the secondary beam sticks with respect to the friction interface. The measured displacement response when friction was applied to the system is shown in **Figure 22** and **Figure 23** for the case of intermediate and high friction respectively.

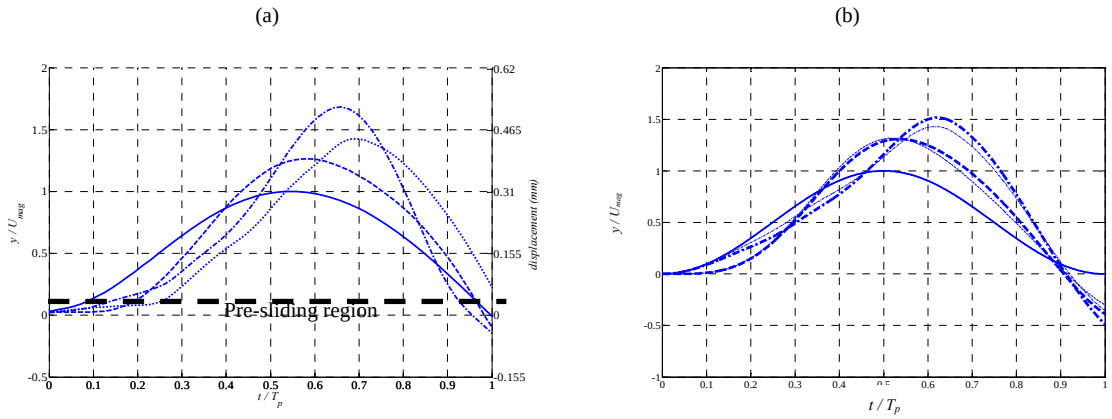

Figure 22: Displacement response of the thin secondary beam system with intermediate friction. (a) Measured. Solid line: Base input. Dash line: Response at the end of the primary beam (sensor 2). Dash dot line: Response at the end of the secondary beam (sensor 3). Dot line: Response at the end of the secondary beam (sensor 4). (b) Simulation with intermediate Coulomb friction. Solid line: Base input. Dash thick line: Primary mass response, $\hat{F} = 0.39$. Dash thin line: Primary mass response, $\hat{F} = 0.48$. Dash dot thick line: Secondary mass response, $\hat{F} = 0.39$. Dash dot thin line: Secondary mass response, $\hat{F} = 0.48$.

For the case of intermediate friction (**Figure 22**), the response at the two ends of the secondary beam were slightly different. The difference in the response until a normalised time of 0.5 is small and it subsequently increased slightly. This is as expected from the previous free vibration experiment which shows that the friction did vary slightly throughout the motion and may influence the level of friction at each end of the secondary beam.

There are also two other identified sources of discrepancy. The first one is the existence of pre-sliding region when the motion starts. During this experiment, the base input displacement range generated from the shaker is quite small, roughly less than 1 mm. The pre-sliding region occurs when the displacement is very small often between 1 and 10 μm [26]. Hence, in the case of small displacement, the pre-sliding region is significant in describing the behaviour of the system. This behaviour is demonstrated until normalised time of 0.25. The behaviour shows that before gross slip occurs, there is local sliding in the contact. The microscopic behaviour can be explained by the interaction between the contact asperities which behave as welded junctions and the shearing that tends to break them [27]. The Coulomb friction model has its limitation in describing the motion within this region [26]. Andersson et al explained that there are other friction models which are more suitable to describe the motion within the region. The models describe, for small displacement, that friction increases with displacement until it reaches the level which can be considered to be the Coulomb sliding friction force. Other publications also discussed how the friction increase depends upon the stationary contact time before gross slip [27, 28, 29].

The second source of discrepancy is a soft secondary spring, which could cause the secondary mass to stick for slightly higher levels of friction. From the parameter estimation, the secondary stiffness is only about half of the primary stiffness. From the simulation, the range of the sliding region for the secondary mass before it sticks is quite small. Any small change in friction could cause the secondary mass to stick and cause significant difference in the secondary mass response.

The measured response is then compared with the simulation with non-dimensional friction set as $\hat{F}$ =0.39 and $\hat{F}$ =0.48, which are the estimated friction values calculated from the previous section. In the simulation, the system reaches its peak displacement before the experiment. This shows that Coulomb friction model only appears to be appropriate after non dimensional time of about 0.25, where the displacement at the end of the secondary beam is significantly greater than 10 μm. At this point, the friction has increased to the level of the Coulomb sliding friction force and gross slip has started. However, the experimental and simulation results are still in good agreement with each other and the overall behaviour can still be predicted using simulation with reasonable accuracy.

(a) (b)

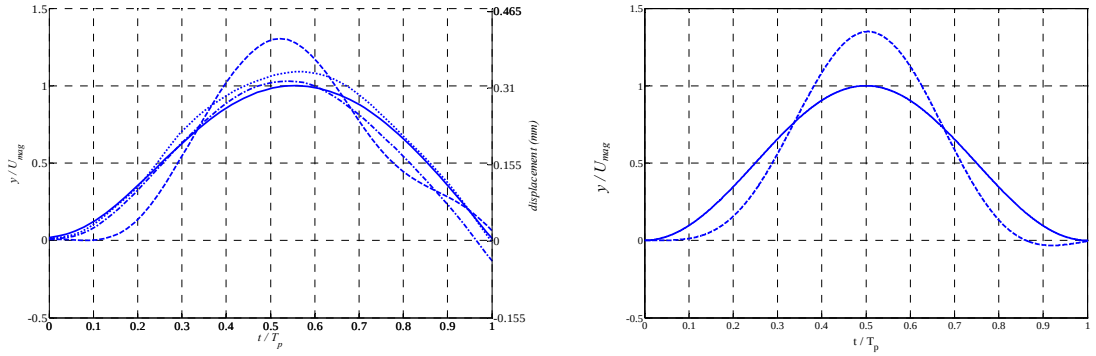

Figure 23: Displacement response of the thin secondary beam system with high friction. (a) Measured. Solid line: Base input. Dash line: Response at the end of the primary beam (sensor 2). Dash dot line: Response at the end of the secondary beam (sensor 3). Dot line: Response at the end of the secondary beam (sensor 4). (b) Simulation with high Coulomb friction. Solid line: Base input and response of the secondary mass. Dash line: Response of the primary mass.

For the case of high friction the end of secondary mass stuck and moved with the base as expected. From the experiment, both ends of the secondary beam had same displacement as the base. The measured response is also in good agreement with the predicted results from the simulation.

The results for different levels of friction were compared to see the effect of friction in reducing the displacement and velocity response of the primary mass during the shock. The results are shown in **Figure 24**. From the results, the intermediate friction produces the smallest primary mass response. It matches the prediction from the simulation, where the smallest response is produced when the secondary mass slides on the friction interface instead of fully sticking. The reduction is small in this case because the choice of the T beam which produced a secondary spring that is softer compared to the primary spring in the two degree of freedom model. An increase in the secondary spring value will produce more reduction in the response of the isolated mass, which will be shown in the next section.

(a) (b)

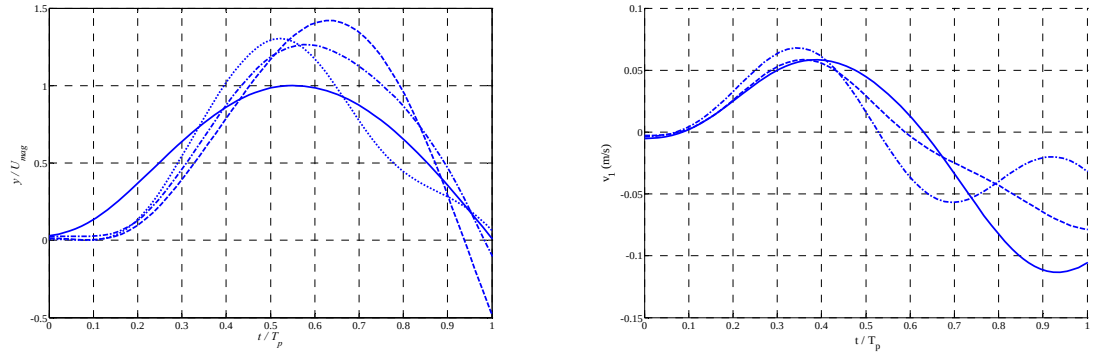

Figure 24: (a) Comparison between measured displacement responses at the end of the primary beam with different levels of friction for the case of the thin secondary beam. (b) Comparison between measured velocity responses at the end of the primary beam with different levels of friction for the case of the thin secondary beam. Solid line: Base input. Dash line: No friction. Dash dot line: Intermediate friction. Dot line: High friction.

5.7 Validation for the case when friction is applied (Thick secondary beam with friction : under base excitation)

Similar to the case of the thin secondary beam, two levels of friction were also applied to the system with a thick secondary beam, namely intermediate and high friction. The measured displacement response when friction was applied to the system is shown in **Figure 25 (a)** and **Figure 25 (b)** for the case of intermediate and high friction respectively. For validation, the displacement of a single degree of freedom model is also plotted in the same figure. The simulation using the single degree of freedom model was performed

with two estimated friction values, $\hat{F}$=0.2 and $\hat{F}$=0.3 for the case of intermediate friction. From **Figure 25**, the measurements results are very close to the predicted response using the single degree of freedom model.

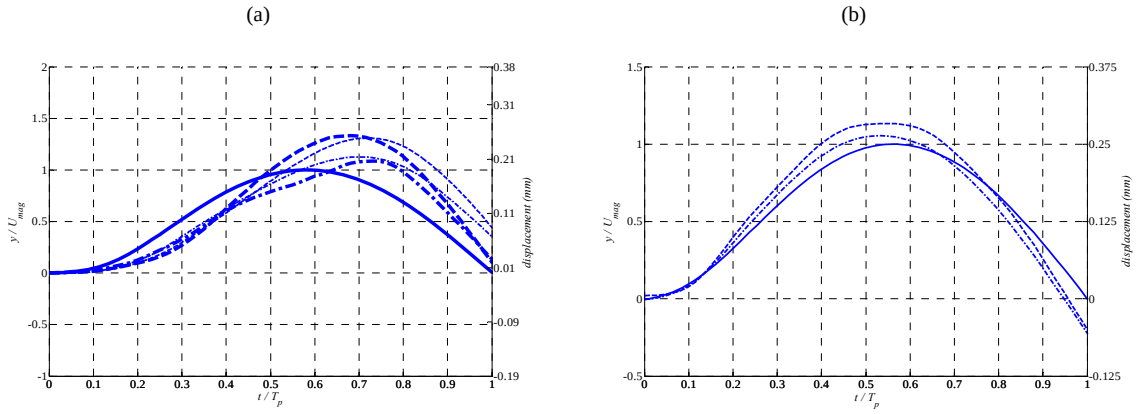

Figure 25: (a) Displacement response of the thick secondary beam system with intermediate friction. Thick solid line: Base input. Thick dash line: Measured response at the end of the primary beam. Thick dash dot line: Measured response at the end of the secondary beam. Thin dash line: ODE simulation mass response, $\hat{F}$=0.2. Thin dash dot line: ODE simulation mass response, $\hat{F}$=0.3. (b) Displacement response of the thick secondary beam system with high friction. Solid line: Base input. Dash line: Response at the end of the primary beam. Dash dot line: Response at the end of the secondary beam.

When friction is applied and increased, there is a reduction in the normalised displacement response of the system as expected. The measured displacement response for different levels of friction is shown in **Figure 26**. The normalized displacement response decreased from 1.7 to 1.33 which is about 21.8% reduction with intermediate friction. As the friction was further increased, the normalised displacement response was further reduced to 1.13, which is about 33.5% reduction in comparison to the case of no friction.

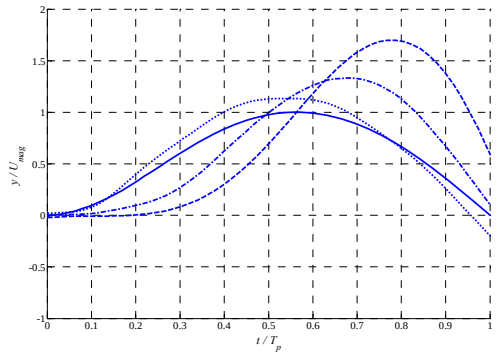

Figure 26: Comparison between measured displacement responses at the end of the primary beam with different levels of friction for the case of the thick secondary beam. Solid line: Base input. Dash line: No friction. Dash dot line: Intermediate friction. Dot line: High friction.

5.8 Comparison between the response of the thin and thick secondary beam

Table 4 shows the measured response of the system with either thin or the thick secondary beam. From inspection of the results presented in the table, a smaller displacement response of the end of the primary beam is produced when the thick secondary beam is used. The results matched the prediction from **Section 4.1**, as more displacement reduction was obtained for the primary mass when a stiffer secondary spring is used in the two degree of freedom model with friction. This is because a stiffer secondary spring is required for the friction effect to be transferred to the primary mass. The highest reduction obtained when the secondary spring becomes very rigid as per single degree of freedom system. Although the choice of stiffer secondary spring produced a smaller displacement response, it creates a sharp transition and acceleration discontinuity as discussed in **Section 4.2**.

Categories	Thin secondary beam			Thick secondary beam	
	End of primary beam maximum displacement	End of secondary beam maximum displacement		End of primary beam maximum displacement	End of secondary beam maximum displacement
No friction	1.42	Sensor 3	1.96	1.7	1.71
		Sensor 4	2.05		
Intermediate friction	1.26	Sensor 3	1.68	1.33	1.09
		Sensor 4	1.43		
High friction	1.31	Sensor 3	1.03	1.13	1.06
		Sensor 4	1.09		

Table 4: Comparison between the maximum displacement responses of the systems with thin and thick secondary beams. The maximum displacements are normalized with respect to the maximum base input displacement.

In contrast, if the secondary spring is too soft like the case of the thin secondary beam, not much attenuation was obtained in the maximum displacement response which is also illustrated in **Table 4**. This is the reason why the two degree of freedom model was introduced in order to have various values for the secondary spring for an optimum response of both the displacement and acceleration. As discussed in **Section 4.1** and **4.2**, there is an intermediate optimum value where significant maximum displacement reduction and smoother acceleration can be produced.

From **Section 4.1** and **4.2**, the smallest maximum displacement was obtained when the intermediate friction values used, while the mass slides instead of sticking on the friction interface. This has been displayed by the case of the thin secondary beam. However, it is not obvious in the case of the thick secondary beam where more friction should be used to observe this behaviour.

6. Conclusions

The friction element has been shown to possess a good property in producing isolation during the shock and suppressing the residual vibration after the shock. This is because, the force transmission across the friction element is only dependent upon the direction of the relative velocity across it instead of magnitude of the relative velocity. The issue with friction is it creates unsmooth acceleration response at the point where the motion starts and changes in the direction of motion. Therefore, a two degree of freedom model was introduced where friction is applied to a secondary mass and the primary mass becomes the isolated mass. Both significant maximum displacement reduction and smoother acceleration can be achieved for the primary isolated mass when an intermediate value of the secondary stiffness is used.

The theoretical predictions have been experimentally validated with a test rig designed for the first stage during the shock. The test rig involves the T-beam configuration which closely replicates the response of a lumped parameter two degree of freedom model at low frequencies below 200 Hz. A steel beam attached to the base is used to apply friction on the T-beam configuration. Validation of the system produced comparable results to the model with explainable differences. Among the differences are slight dissimilarity between the experimental and theoretical versed sine input, the suitability of the Coulomb friction to model a system with small displacements, the possibility of friction changes as the friction surface moves and the possibility of friction differences between the two ends of the secondary beam.

The novel strategy to suppress the residual vibration after the shock with the proposed two degree of freedom model was studied and discussed theoretically [11]. However, no experimental verification has been done and it may be interesting topic of future research. There is limitation on the electrodynamic shaker system where the base still oscillates after the shock and applies a significant input to the test rig [11]. The base needs to stop vibrating completely after the shock input to represent the ideal condition and this is dependent upon the amount of inertia and damping present in the shaker-rig system.

7. Acknowledgements

The authors wish to express their gratitude to the Majlis Amanah Rakyat (MARA) for the financial support of the research programme reported herein.

References

[1] C.M.Harris and C.E.Crede, *Shock and Vibration Handbook*. 4 ed, ed. C.M.Harris and C.E.Crede. 1995, New York: McGraw-Hill.

[2] C.T.Morrow, *Shock and Vibration Engineering*. 1963, New York: John Wiley and Sons.

[3] R.S Ayre, *Engineering Vibrations*, McGraw-Hill, New York, 1958

[4] D.F.Ladezma Ramirez, N.S.Ferguson, and M.J.Brennan, *Shock isolation using an isolator with switchable stifness.* Journal of Sound and Vibration, 2011.

[5] T.P.Waters, Y.Hyun, and M.J.Brennan, *The effect of dual rate suspension damping on vehicle response to transient road inputs.* Journal of Vibration and Acoustics, 2009. **131**.

[6] Y.Hyun, *The effect of suspension damping on vehicle response to transient road inputs*, MPhil thesis Institute of Sound and Vibration Research. 2005, University of Southampton: Southampton.

[7] J.P.D.Hartog, *Mechanical Vibrations*. 4 ed. 1985, New York: Dover Publications, INC.

[8] J.P.D.Hartog, *Forced vibrations with combined viscous and Coulomb damping.* Philosophical Magazine, 1930. **9**(59): p. 801-817.

[9] M.S.Hundal, *Response of a base excited system with Coulomb and viscous friction.* Journal of Sound and Vibration, 1979. **64**(3): p. 371-378.

[10] A.A.Ferri, *Friction damping and isolation systems.* Journal of Vibration and Acoustics, 1995. **117(B)**: p. 196-206.

[11] M.I.Ismail, *Shock isolation systems incorporating Coulomb friction*, PhD thesis Institute of Sound and Vibration Research. 2012, University of Southampton: Southampton.

[12] S.Timoshenko, D.H.Young, and W.Weaver, *Vibration Problems in Engineering*. 1974: John, Wiley and Sons Inc.

[13] C.A.Mercer and P.L.Rees, *An optimum shock isolator.* Journal of Sound and Vibration, 1971. **18**(4): p. 511-520.

[14] R.P.Nanda, P.Agarwal and M.Shrikhande, *Suitable friction sliding materials for base isolation of masonry buildings.* Journal of Shock and Vibration, vol. 19, no. 6, pp. 1327-1339, 2012. doi:10.3233/SAV-2012-0675.

[15] J.A.Kulkarni and R.S. Jangid, *Effect of superstructure flexibility on the responnse of base isolated structures.* Journal of Shock and Vibration, 10 (2003) 1-13.

[16] P.Castaldo and E.Tubaldi, *Influence of FPS bearing properties on the seismic performance of base-isolated structures.* Earthquake Engineering and Structural Dynamics, 2015. *44: 2817–2836. doi: 10.1002/eqe.2610.*

[17] L.Gaul and J.Becker, *Reduction of Structural Vibrations by Passive and Semiactively Controlled Friction Dampers.* Journal of Shock and Vibration, vol. 2014, Article ID 870564, 7 pages, 2014. doi:10.1155/2014/870564

[18] S.Andersson, A.Soderberg, and S.Bjorklund, *Friction models for sliding dry, boundary and mixed lubricated contacts.* Tribology International, 2007. **40**: p. 580-587.

[19] G.J.Stein, R.Zahoransky, and P.Mucka, *On dry friction modelling and simulation in kinematically excited oscillatory systems.* Journal of Sound and Vibration, 2008. **311**: p. 74-96.

[20]N.Andreaus and P.Casini, *Dynamics of friction oscillators excited by a moving base and/or driving force.* Journal of Sound and Vibration, 2001. **245**: p. 685-699.

[21]N.Mostaghel and T.Davis, Representations of Coulomb friction for dynamic analysis. Earthquake Engineering and Structural Dynamics, 1997. 26: p. 541-548.

[22] I.Lopez and H.Nijmeijer, *Prediction and validation of the energy dissipation of a friction damper.* Journal of Sound and Vibration, 2009. **328**: p. 396-410.

[23] R.J.Allemang and D.L.Brown, *A correlation coefficient for modal vector analysis*, in *Proceedings of the 1st International Modal Analysis conference (IMAC)*. 1982: Orlando, Florida

[24] M.I.Friswell and J.E.Mottershead, *Finite Element Model Updating in Structural Dynamics*. 1995, Dordrecht: Kluwer Academic Publishers.

[25] D.F.L.Ramirez, *Shock isolation using switchable stiffness*, PhD thesis *Institute of Sound and Vibration Research*. 2008, University of Southampton: Southampton. p. 205.

[26] S.Andersson, A.Soderberg, and S.Bjorklund, *Friction models for sliding dry, boundary and mixed lubricated contacts.* Tribology International, 2007. **40**: p. 580-587.

[27] J.F.Ferrero and J.J.Barrau, *Study of dry friction under small displacements and near zero sliding velocity.* Wear, 1997. **209**: p. 322-327.

[28] J.F.Ferrero, et al., *Analysis of a dry friction problem under small displacements: application to a bolted joint* Wear, 2004. **256** p. 1135-1143

[29] E.Rabinowicz, *The intrinsic variables affecting the stick-slip process.* Proc.Phys Soc., 1958. **71**: p. 668-675.